MOLECULES, GRAINS, AND SHOCKS: A COMPARISON OF CO, H I, AND *IRAS* DATA

CARL HEILES, WILLIAM T. REACH, AND BON-CHUL KOO
Berkeley Astronomy Department, University of California

ABSTRACT

We have compared the IR and H I properties, and CO content, of a set of 26 isolated, degree-sized interstellar clouds. The comparisons offer some conclusions concerning the effects of kinematics on molecular content and grain size distribution, although these conclusions are provisional because of the small sample. The departure of S_{100}/N_{HI}, where S_{100} is the 100 μm surface brightness, from the theoretically predicted value is a measure of the H_2 content of clouds. This is confirmed by the detection of CO in clouds with large S_{100}/N_{HI}. Even clouds with low column density, $\sim 2.4 \times 10^{20}$ H-nuclei cm^{-2} or less, may contain more H_2 than H I, in contrast to results obtained from UV absorption line studies. The $[H_2/H\ I]$ ratio is large only for quiescent clouds.

The dependence of S_{60}/S_{100} on velocity implies that fast shocks preferentially destroy large grains or produce small grains, or both. The marginally defined dependence of S_{12}/S_{100} on velocity, if real, probably implies that very small grains (VSGs) are formed in shocks in the 10–20 km s^{-1} velocity range, and destroyed at slightly higher velocities. Two neighboring clouds have been affected by the same shock, but with different degrees of completion; comparison of these two allows us to estimate a time scale for VSG formation. Nearly *all* clouds, independently of kinematics, appear to contain VSGs.

Some members of our cloud sample emit more power in the *IRAS* 12 μm band than in the 100 μm band. Such clouds must have very large fractions of their total carbon in the form of polycyclic aromatic hydrocarbons (PAHs), if VSGs are exclusively PAHs. Finally, the absence of correlation of S_{12}/S_{100} with S_{60}/S_{100} implies that VSGs are not formed preferentially from the breakup of large grains.

Subject headings: interstellar: abundances — interstellar: grains — interstellar: molecules — radio sources: 21 cm radiation — shock waves

I. INTRODUCTION

We have isolated a set of *IRAS*–detected interstellar clouds for detailed study. These are unlike ordinary "interstellar cirrus," which is distributed as ordinary H I gas and is extended over large regions (Boulanger, Baud, and van Albada 1985). Instead, they are isolated clouds whose size is of order one degree. Most of these blobs are barely noticeable on photographs of H I such as presented by Colomb, Pöppel, and Heiles (1980). We became aware of their existence only after examining the *IRAS* sky prints. This paper discusses 26 of these clouds, a large fraction of the total sample observable from the northern hemisphere. In four of these 26 clouds there are separable structures, and we have made independent measurements at two positions; we treat these measurements as independent points.

Some of our clouds appear in other authors' lists. G90+38.8 is in complex number 26 of high-latitude CO clouds of Magnani, Blitz, and Mundy (1985). It is the "Draco cloud," and has been studied in detail in a series of papers by Mebold and collaborators (see Mebold *et al.* 1985), by Johnson (1986), and by Odenwald and Rickard (1987). G192.3−67.9, G229.0−66.1, G228.0−28.6, and G230.1−28.4 appear in the list of comet-like *IRAS* clouds of Odenwald and Rickard (1987).

We regard our clouds as typical examples of the cloud component of the interstellar medium, which should be distributed in z as are other interstellar clouds. This implies that the typical distance should be ~100 pc (Magnani, Blitz, and Mundy 1985). Because most of our clouds are located at high Galactic latitude, the |z|-height should not be much smaller.

For G90.0+38.8, Mebold *et al.* (1985) derive a distance of 800 pc from a combination of star counts and extinction inferred from CO data. Their derived distance depends sensitively on the extinction, which in turn depends on the detailed way in which the CO observations are interpreted. We believe that there is a large uncertainty in the distance to G90.0+38.8.

We have made measurements of these clouds in the 21 cm H I line and the 2.6 mm $J = 1–0$ CO line, and we have studied the infrared emission. The clouds exhibit a remarkable diversity of both kinematic and IR properties. This diversity allows us to obtain some conclusions concerning the effects of shocks upon the H_2 content and the grain size distribution. Section II describes our methods to derive the infrared emission in the four *IRAS* bands, and presents the results; § III describes our H I observations. Section IV puts the two data sets together and describes the implications for models of interstellar grains.

II. INFRARED PROPERTIES FROM *IRAS* DATA

To compare accurately the IR emission and the 21 cm emission, we determined the "position-switched" 100 μm emission from each cloud by integrating the *IRAS* sky images at the positions observed with the radio telescope (§ III), weighting the integrations with the beam shape of the radio telescope (taken to be a Gaussian with HPBW = 36'). For most clouds we used *IRAS* HCON1 data. However, some clouds were poorly sampled by the HCON1 data; for these we used either the HCON2 or HCON3 data sets. For two clouds of particular interest, we used all three HCON data sets.

To obtain intensities in each *IRAS* band for the purposes of deriving the spectrum, we derived average surface brightnesses

within an appropriately chosen rectangular box with respect to the background in the immediate vicinity of the cloud. Removing the background is crucial, because the background emission is always larger than the emission from the cloud itself. This effect is most serious at 12 and 25 μm, where the Zodiacal emission constitutes ~99% of the total emission. Over the few-degree scale of interest here, the Zodiacal emission adds a slowly varying vackground which can be removed easily by fitting a smooth surface with a low-order polynomial. More difficult is an instrumental effect: the *IRAS* maps were made by repeatedly scanning the satellite over the sky, changing the scan direction by 1' or so from one scan to the next. The sky images were built up by combining these scans. The scans have slightly different offsets and different solar elongations, which leads to pronounced "stripes" in the sky images: each stripe is a different scan with a different instrumental contribution to the background.

The stripes cannot be easily removed. We have minimized their effect by using the following procedure. We choose the size of the rectangular box over which we wish to integrate. We note the direction of the satellite scans on the sky image, and determine the particular line on the sky image, parallel to the scan direction, that intersects the center of the cloud of interest. We calculate the average surface brightness within the box as a function of position along the line, and examine the resulting one-dimensional distribution with astronomical spectral-

analysis software, which allows us to remove the zodiacal background with a smooth one-dimensional polynomial fit and to easily determine the brightness of the cloud relative to its surroundings. It also allows a realistic assessment of the error of the photometry.

Figure 1 exhibits the images of G228.0−28.6 and G230.1−28.4, two important clouds which are discussed below in § IV*a*, and illustrates the application of the technique. Figure 2 depicts the results of the one-dimensional scans across these clouds. Note that Figure 1 shows only a fraction of the scan length depicted in Figure 2. Table 1 presents the basic IR data on all clouds, together with the derived intensities and their errors. In all cases, the average surface brightness is denoted by the symbol S, with a subscript equal to the wavelength of the *IRAS* band in μm, and our units are MJy sr^{-1}. No color corrections have been applied; the conversion from *IRAS* flux to flux density assumes a ν^{-1} spectrum.

For each *IRAS* band, the quoted error on S was obtained from angular fluctuation in the background near the cloud. Angular fluctuations arise from three sources: real fluctuations in the diffuse interstellar emission, fluctuations in the zodiacal emission, and instrumental errors and noise. The zodiacal component usually varies smoothly on angular scales of several degrees; it can usually be represented by least-squares parabolic fit and subtracted in an unambiguous way, as was done for Figure 2. Interstellar fluctuations are less easily
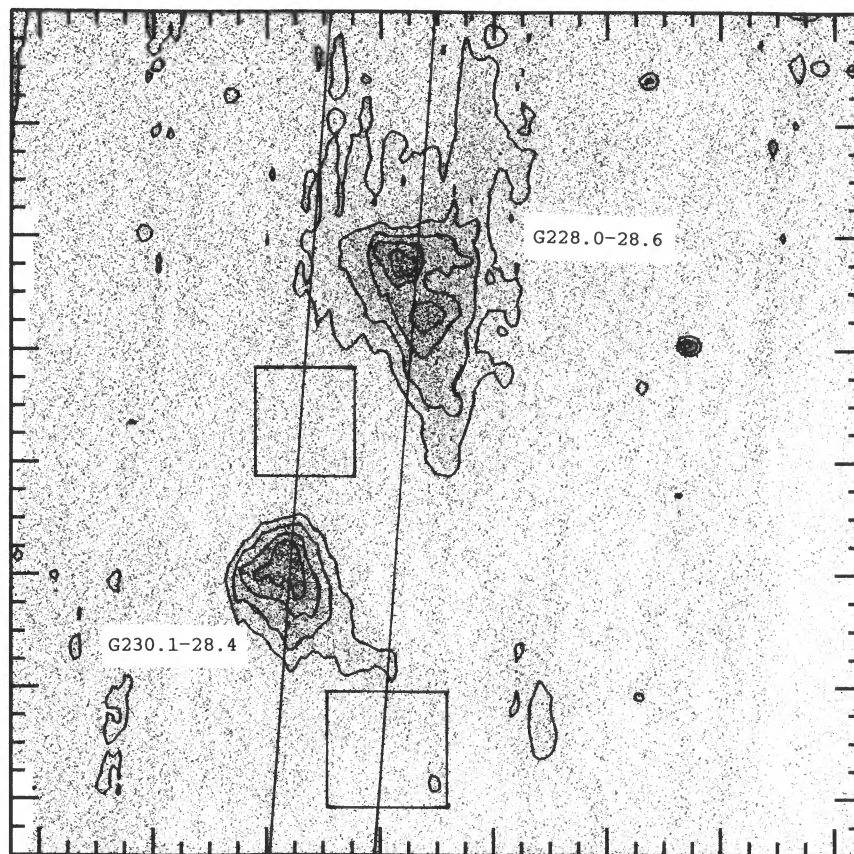
FIG. 1.—100 μm image of clouds G228.0−28.6 (*top*) and G230.1−28.4 (*bottom*). The straight lines are parallel to the *IRAS* scan direction and are the lines along which the rectangular boxes (shown) were moved in generating the one-dimensional scans of *IRAS* surface brightnesses, from which the intensities of the clouds in the four *IRAS* bands were determined. This image is a small (~10% in area) section of *IRAS* SKYFLUX Plate 148, HCON 2. Major tick marks on both axes are separated by 40' (20 pixels), minor tick marks by 10' (5 pixels).
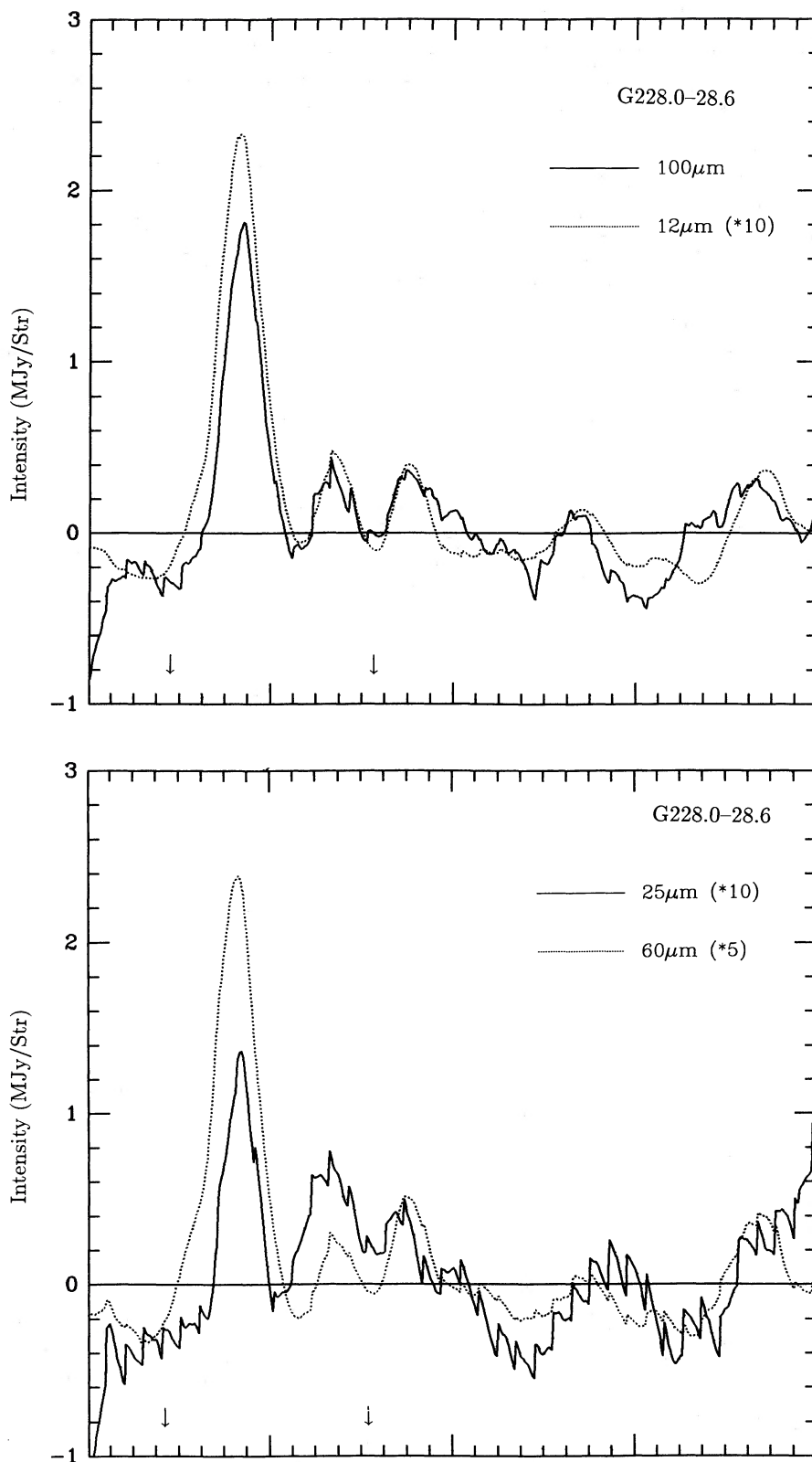
FIG. 2.—One-dimensional scans of the *IRAS* data along the lines shown in Fig. 1, integrated within the rectangular boxes. Vertical axes are labeled in MJy/Sr. Horizontal axes correspond to distance along the scan; tick marks are separated by ∼30′. A parabola has been least-squares fit to the entire length of each scan over the *full* extent of plate 148, except for the portion occupied by the clouds and subtracted from the scans before plotting. The portion of the scan pictured on Fig. 1 is indicated by the arrows. (*a*) G228.0−28.6, (*b*) G230.1−28.4. *Top panels:* solid line, 12 μm, multiplied by 10; dotted line, 100 μm. *Bottom panels:* solid line, 25 μm, multiplied by 10; dotted line, 60 μm, multiplied by 5.
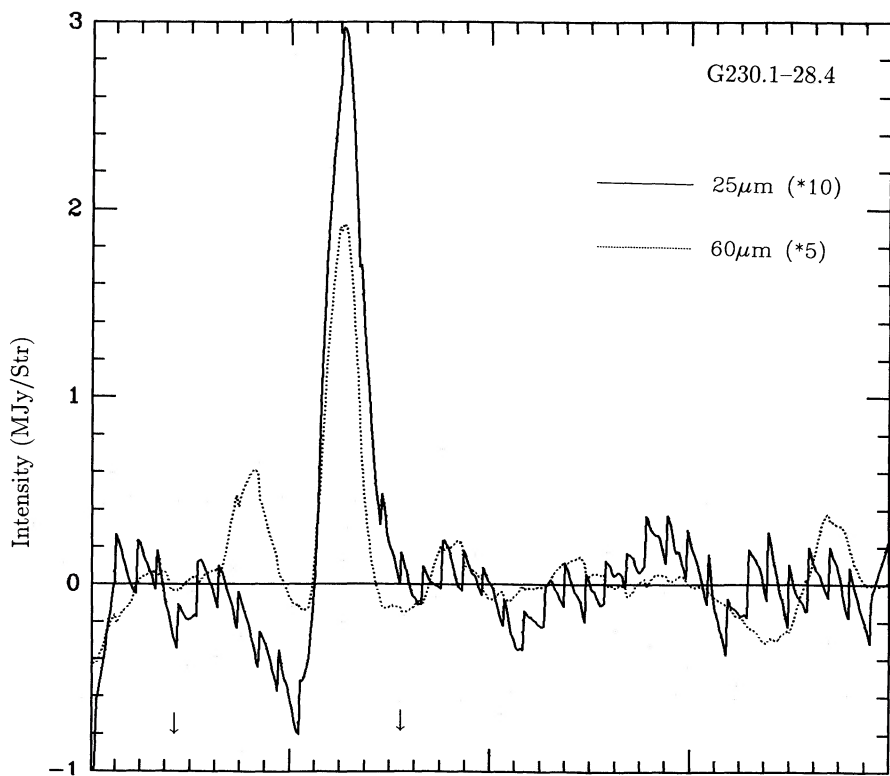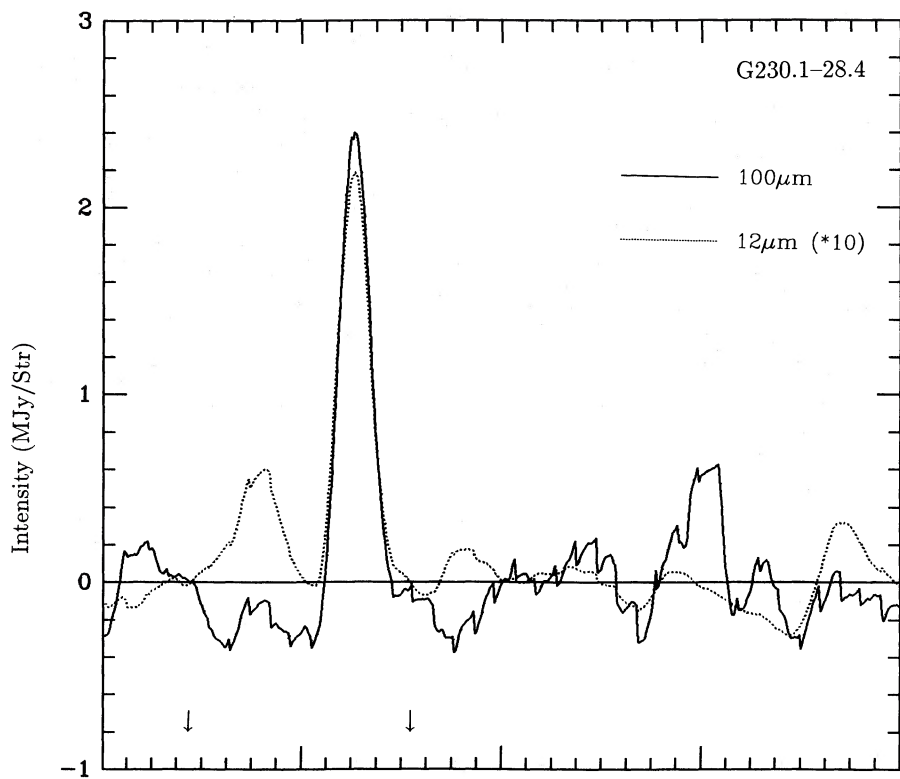
FIG. 2b

TABLE 1

IR PROPERTIES OF CLOUDS

Cloud	R.A.	Decl.	DEL R.A.[a]	DEL Decl.[a]	Box Size[b]	HCON	$S(100)$	$S(60)/S(100)$	$S(25)/S(100)$	$S(12)/S(100)$
G101.9−62.0	$00^h10^m00^s$	$-01^d00'00''$	00^m00^s	$01^d00'$	40×32	1	1.370	0.317 (0.034)	0.243 (0.051)	0.088 (0.013)
G81.4−77.8	00 15 00	−18 00 00	−05 00	00 00	36×44	1	1.300	0.273 (0.030)	0.066 (0.030)	0.042 (0.013)
G120.1−67.2	00 44 00	−04 40 00	00 00	02 00	36×36	2	2.790	0.249 (0.025)	0.051 (0.028)	0.077 (0.009)
G135.4−68.7	01 07 00	−06 07 00	00 00	02 00	28×72	2	6.670	0.196 (0.005)	0.038 (0.036)	0.052 (0.005)
G192.3−67.9	02 16 00	−17 55 00	−05 00	00 00	32×32	1	1.690	0.226 (0.011)	0.078 (0.012)	0.045 (0.007)
G229.0−66.1	02 37 44	−31 18 45	−06 00	00 00	20×40	1	1.250	0.162 (0.038)	0.106 (0.021)	0.078 (0.015)
G225.6−66.4	02 36 03	−29 55 52	−05 00	00 00	36×36	1	1.140	0.157 (0.029)	0.073 (0.013)	0.071 (0.015)
G243.2−66.1	02 33 03	−37 00 16	−06 00	00 00	60×36	1	1.150	0.178 (0.029)	0.056 (0.025)	0.065 (0.005)
G240.2−65.5	02 37 31	−35 56 45	05 00	00 00	36×44	1	1.110	0.175 (0.024)	0.041 (0.064)	0.057 (0.014)
G228.0−28.6	05 26 09	−24 58 07	−00 22	−01 36	44×44	123	2.440	0.212 (0.030)	0.067 (0.022)	0.086 (0.010)
G230.1−28.4	05 29 50	−26 40 27	−03 32	00 06	36×40	123	1.730	0.191 (0.011)	0.126 (0.024)	0.121 (0.010)
G235.9+38.2	09 43 22	00 45 53	−03 00	−01 36	44×36	1	5.180	0.214 (0.0082)	0.0553 (0.0039)	0.0767 (0.0032)
G235.0+38.7	09 43 30	01 39 43	03 20	01 26	44×48	1	3.920	0.190 (0.012)	0.0449 (0.0015)	0.0721 (0.0024)
G163.9+59.7	10 52 10	47 25 00	03 30	01 00	28×28	1	0.576	0.212 (0.059)	0.073 (0.042)	0.044 (0.041)
G139.6+47.6	10 56 00	66 00 00	07 52	00 48	48×44	1	0.996	0.187 (0.024)	0.073 (0.026)	0.037 (0.015)
G141.1+48.0	10 50 55	65 01 37	−07 15	−00 46	40×40	1	1.160	0.175 (0.020)	0.052 (0.020)	0.029 (0.017)
G135.5+51.3	11 36 00	64 20 00	00 00	01 20	36×36	1	1.750	0.266 (0.022)	0.090 (0.015)	0.052 (0.010)
G137.3+53.9	11 38 00	61 30 00	00 00	01 10	56×40	1	1.230	0.244 (0.036)	0.058 (0.012)	0.052 (0.011)
G135.3+54.5	11 49 00	61 30 00	00 00	01 20	40×48	1	1.640	0.244 (0.017)	0.120 (0.015)	0.036 (0.005)
G149.9+67.4	11 50 00	46 50 00	00 00	01 00	24×28	1	0.187	0.206 (0.055)	0.090 (0.043)	0.070 (0.041)
G249.0+73.7	11 54 00	17 10 00	00 00	02 00	32×32	1	2.390	0.227 (0.069)	0.050 (0.022)	0.076 (0.017)
G124.1+71.6	12 47 00	45 50 00	00 00	01 30	32×20	1	1.250	0.319 (0.020)	0.042 (0.014)	0.060 (0.013)
G107.4+70.9	13 18 00	45 40 00	−05 00	01 00	40×64	1	1.250	0.365 (0.037)	0.066 (0.011)	0.029 (0.007)
G99.3+69.0	13 40 00	47 00 00	09 00	00 00	36×72	1	0.740	0.214 (0.032)	0.017 (0.015)	0.047 (0.015)
G86.5+59.6	14 38 53	49 17 55	−08 00	02 00	60×60	1	2.800	0.334 (0.017)	0.050 (0.014)	0.059 (0.014)
G90.0+38.8	16 44 42	60 15 48	00 00	−01 00	40×32	1	2.410	0.139 (0.012)	0.038 (0.010)	0.037 (0.0055)
G94.8+37.6	16 47 00	64 15 00	−08 00	−01 00	40×32	1	1.100	0.175 (0.017)	0.063 (0.0019)	0.046 (0.010)
G81.2+39.2	16 50 00	53 30 00	00 00	01 00	32×28	1	1.660	0.184 (0.046)	0.046 (0.094)	0.050 (0.042)
G86.0+38.3	16 53 04	57 17 35	00 00	−01 00	36×48	23	1.270	0.299 (0.030)	0.038 (0.012)	0.032 (0.011)
G25.1−67.7	23 08 00	−28 10 00	00 00	−02 00	36×32	2	1.370	0.344 (0.079)	...	0.077 (0.054)

[a] Offsets to reference position.
[b] Box size is in arcmin, R.A. × decl.

treated. They repeat in all four bands, as in Figure 2. For many clouds, the fluctuation level in the surrounding sky is small: it can be reasonably represented by subtracting a least-squares linear or parabolic baseline from the one-dimensional scan over angular scales comparable to that of the cloud on each side of the cloud, and calculating the rm fluctuation level of the residual. However, for some clouds there are large interstellar fluctuations in the vicinity of the cloud, so large that they are clearly not random fluctuations and do not represent the uncertainty in the cloud's intensity. In these cases, not only the estimate of the random fluctuations but also the very definition of the cloud itself is a subjective procedure. We attempted to derive errors in the same way as for isolated clouds, i.e., by calculating the rms fluctuation level over a suitably defined distance in the scan. However, in some instances this distance is shorter than the cloud's diameter. Nevertheless, this distance was never shorter than 40′, which would seem to be adequate for a realistic error estimate.

Errors in the cloud intensity *ratios* were derived directly from the estimated errors (ΔS) by combining them in the appropriate fashion for uncorrelated errors and multiplying 1.36. For example, the error in S_{60}/S_{100} was set equal to 1.36 $\times [S_{60}/S_{100}][(\Delta S_{60}/S_{60})^2 + (\Delta S_{100}/S_{100})^2]^{1/2}$. The factor 1.36 was derived from comparison of different methods of obtaining errors from three independent measurements (the three HCON data sets) of clouds G228.0−28.6 and G230.1−28.4. One method, which we regard as the most realistic estimate of errors in intensity ratios, was obtained from the rms fluctuation in intensity ratios of the three independent estimates. The other utilized the method described above for each individual HCON, and was a factor of 1.36 smaller. The errors for intensity ratios quoted in Table 1 and shown in the figures include this factor of 1.36 and represent our best estimate of the 1 σ errors.

Odenwald and Rickard (1987) have derived the four *IRAS* band intensities for a $34' \times 36'$ area centered on the "Draco Head," which lies only 8′ away from our G90.0+38.8. Their intensity ratios, after removing the 240 K color corrections that they applied, differ from ours and must be multiplied by the approximate factors 1.18, 1.61, and 2.82 to recover our values of S_{60}/S_{100}, S_{25}/S_{100}, and S_{12}/S_{100}, respectively. We do not understand these large discrepancies. It is inconceivable that our measurements are so inaccurate. As noted by Odenwald and Rickard, their S_{12}/S_{100} for Draco is much lower than values obtained for other clouds by other authors. Odenwald and Rickard used extensive image processing, deleting certain Fourier components in the image, to remove the stripes from their *IRAS* images, and we can only assume that this processing has made their results inaccurate.

III. RADIO LINE OBSERVATIONS

We used the 85 foot telescope at Hat Creek Observatory to observe the 21 cm line associated with the clouds. Observations were performed in both position-switched and frequency-switched modes. This allowed us to obtain accurate line profiles both on the cloud and on a nearby reference position, so that we could determine the excess emission associated with the cloud. Figure 3 illustrates these profiles for the clouds G228.0−28.6 and G230.1−28.4, the clouds shown in Figure 1. As discussed above, we derived 100 μm data that correspond
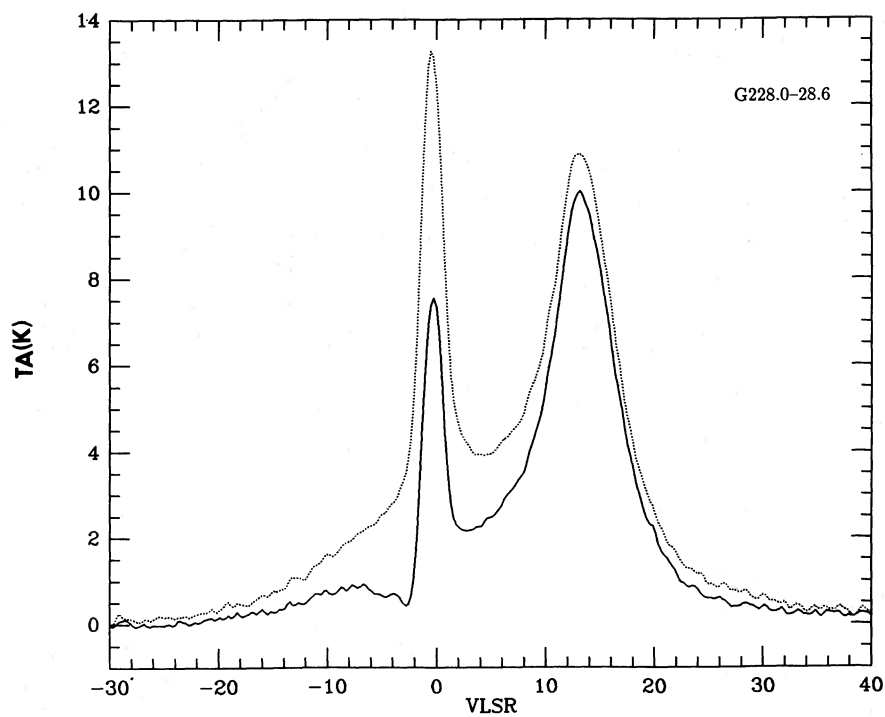
FIG. 3a
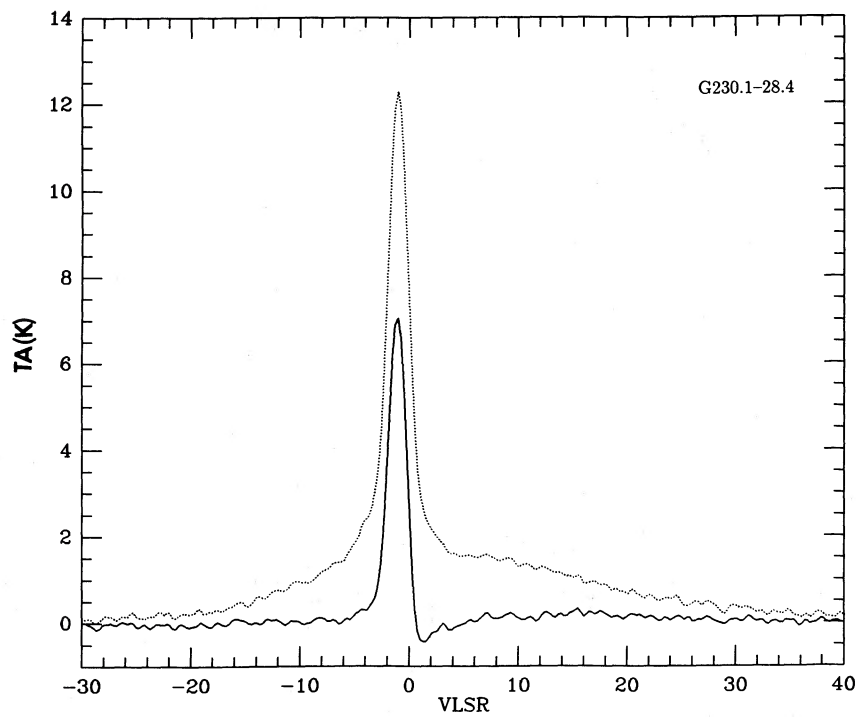
FIG. 3b

FIG. 3.—21 cm line profiles for the two clouds shown in Fig. 1. *Solid lines:* position-switched profiles. *Dotted lines:* frequency-switched profiles on the clouds. (a) cloud G228.0 − 28.6, (b) cloud G230.1 − 28.4.

to these " on " and " off " 21 cm line measurements. Every reference position was located close to the cloud, never more than 2° away, in a direction chosen to minimize the cloud's contribution to the infrared emission. The references positions are given in Table 1.

The telescope was equipped with a dual-channel cooled FET front end, which provided an overall system temperature on cold sky of ~ 55 K, and a 1024 channel autocorrelator. Observations were taken with two bandwidths, 5 and 1.25 MHz. These provided total velocity coverage of 1060 and 265 km s^{-1}, respectively, and resolutions (after Hanning smoothing) of 4.1 and 0.5 km s^{-1}, respectively.

The position-switched profiles were treated in two ways. First, they were fitted with one or more Gaussian components, as many as were required for a reasonable fit. Second, the total H I content was determined by a straight integration under the position-switched profile. Table 2 lists all Gaussians required to obtain a reasonably accurate fit to the line profile of each cloud. Specifically, only Gaussian components whose peak antenna temperatures are larger than 10% of the most intense Gaussian are included. Note that the peak antenna temperature of a component is proportional to its H I column density divided by its velocity width.

Many clouds required more than one Gaussian component. We are immediately faced with the question of whether these multiple components are significant, because H I exists all over the sky and the comparison of arbitrarily chosen neighboring positions almost always produces a nonzero position-switched profile. This question can be answered in a statistical sense: if the multiple Gaussians are associated with unrelated H I that happens to lie along the same line of sight, then about half of the multiple Gaussians should be negative. In fact, most Gaussian components are positive: neglecting the components with very high negative velocities (see below), 14 clouds have multiple Gaussians, and only three clouds have negative Gaussian components. Thus, with 97% confidence, most but not all of our multiple Gaussian components really are associated with the cloud of interest.

This conclusion is corroborated by examination of the Heiles and Habing (1974) position-velocity contour plots for these clouds. In nearly all cases, peaks in the contours at different velocities correspond closely in position. Occasionally, the association is dramatic: the best example is cloud G86.5 + 59.6, which appears on page 263 of Heiles and Habing (1974). The H I spectra themselves provide evidence for a dynamical interaction: there is a weak " bridge " of 21 cm line emission between the -39 and 1 km s^{-1} velocities of the two narrow components listed in Table 2. This broad, weak emission is associated with G86.5 + 59.6, even though we specifically excluded such emission from Table 2. This shows that the complete and correct treatment of H I emission from *IRAS* clouds requires a much more comprehensive and detailed treatment than we have performed herein; we reserve this effort for a future paper.

In contrast, sometimes we consider that there is not an association. For G149 + 67.4 the -52.9 km s^{-1} component is spread over large angles and does not peak at the same position as the -6.3 km s^{-1} component. For this cloud, we ignore the presence of the second (very low column density) Gaussian at -52.9 km s^{-1}.

In two cases, G94.8 + 37.6 and G81.2 + 39.2, there are Gaussian components having velocity with respect to the local standard of rest (V_{LSR}) of -178 and -139 km s^{-1}, respectively.

The association of such high velocity components with the clouds would be very interesting. However, there is a significant probability that the association is not real, because high-velocity clouds cover large areas of the sky in this vicinity (Verschuur 1975). We have therefore discounted this apparent association, although we do reserve its further investigation for the future.

For most clouds with multiple Gaussians, then, we conclude the associations are real and that the kinematics of the gas is correspondingly complicated. The multiple Gaussian components are centered at significantly different velocities, of order 10 km s^{-1} and ranging up to 400 km s^{-1}. For clouds with single Gaussians, the velocity widths indicate the macroscopic velocities inside the cloud. These widths (FWHM) range up to 10 km s^{-1}.

In the following sections, we compare the IR and H I properties of the clouds. For clouds characterized by multicomponent Gaussians, we have reduced the information into a single " condensed Gaussian," whose properties are given in Table 2. We used the following rules for doing so. First, if a Gaussian had a column density smaller than 10% of the column density in the strongest Gaussian component, we disregarded it because such small variations might well arise by chance (this criterion also automatically excludes components having negative column densities). Second, for the clouds characterized by multicomponent Gaussians, we set the velocity width DELTAV of the condensed Gaussian equal to the largest difference between the V_{LSR}'s of the individual Gaussians, or to the largest FWHM, whichever value was larger; and for all clouds represented by single Gaussians, DELTAV was taken equal to the FWHM. The idea is to make DELTAV a measure of the velocity differences within the cloud. Third, the V_{LSR} of the condensed Gaussian was set equal to that of the Gaussian component containing the largest H I column density. Finally, the column density N_{HI} of the condensed Gaussian was set equal to the sum of the N_{HI}'s of the individual Gaussians included, as determined by the above rules. The application of this set of rules is also shown in Table 2. The condensed Gaussians were used in the plots and statistical discussions below.

For the CO observations, we used the 12 m NRAO telescope on Kitt Peak.[1] In the present paper, we only summarize these data in Table 2. They will be discussed in detail in a forthcoming paper. Table 2 shows that a significant fraction of the clouds exhibit CO emission; CO velocities range from -45 to $+8$ km s^{-1}. In most cases, the CO velocity is the same as that of one of the H I components, but not always the strongest H I component. In two cases, G235.9 + 38.2 and G25.1 $-$ 67.7, the CO velocity does not match that of an H I component. In G235.9 + 38.2 there are several H I components, and the CO may exist at a velocity between two colliding components. However, in G25.1 $-$ 67.7, there is only one H I velocity component, and the CO velocity differs from the H I velocity by 6 km s^{-1}. We reserve the investigation of this intriguing situation for a later paper.

IV. DISCUSSION

a) G230.1 $-$ 28.4 and G228.0 $-$ 28.6: Two Shocked Clouds

G230.1 $-$ 28.4 has a very narrow DELTAV and a small $|V_{LSR}|$. Nevertheless, we believe that, *in the recent past*, low-

TABLE 2

H I GAUSSIAN COMPONENTS AND CO VELOCITIES[a]

	DELTAV (km s^{-1})	N (H I) 10^{20}	V_{LSR} (km s^{-1})	N (H I, total)[b] 10^{20}	CO (km s^{-1})
G101.9 − 62.0	3.9	0.25	4.1	...	...
	3.1	0.05	−3.1	...	...
	12.4	0.17	−11.2	...	...
CG	15.3	0.47	4.1	0.48	3
G81.4 − 77.8	5.2	0.77	−8.2	0.85	not observed
G120.1 − 67.2	4.1	1.23	−8.1	...	...
	31.3	0.82	−14.3	...	...
	14.5	0.50	−7.6	...	...
CG	31.3	2.55	−8.1	2.53	−14[c]
G135.4 − 68.7	5.7	2.14	−5.0	...	...
	2.7	0.20	−10.2	...	...
CG	5.7	2.34	−5.0	2.76	not observed
G192.2 − 67.9	3.5	0.78	3.2	...	...
	4.9	0.20	−9.2	...	...
	9.1	0.31	0.9	...	...
CG	12.4	1.29	3.2	1.25	no CO
G229.0 − 66.1	4.1	0.90	−0.4	0.93	no CO
G225.6 − 66.4	3.7	0.30	0.6	0.15	1
G243.2 − 66.1	3.1	0.80	−5.3	0.43	no CO
G240.2 − 65.5	3.7	0.72	−3.9	0.53	no CO
G228.0 − 28.6	5.6	0.77	13.3	...	...
	2.0	0.28	−0.6	...	...
	18.0	1.31	11.0	...	...
CG	18.0	2.36	11.0	2.62	0
G230.1 − 28.4	1.8	0.28	−1.4	0.35	1
G235.9 + 38.2	5.3	1.73	11.1	...	...
	7.3	1.28	4.6	...	...
	4.8	0.33	−5.2	...	...
CG	16.2	3.34	11.1	3.10	8
G235.0 + 38.7	6.3	2.72	9.5	...	...
	7.0	0.58	−6.3	...	...
CG	15.7	3.30	9.5	3.43	no CO
G163.9 + 59.7	6.2	0.29	−19.0	0.14	no CO
G139.6 + 47.6	5.5	0.76	−12.1	0.91	no CO
G141.1 + 48.0	6.5	0.93	−12.9	0.94	−14
G135.5 + 51.3	4.9	1.35	−47.2	1.48	no CO
G137.3 + 53.9	4.6	0.91	−48.2	0.95	no CO
G135.3 + 54.5	4.6	1.28	−47.0	1.29	−45
G149.9 + 67.4	6.5	0.29	−6.3	...	...
	2.6[d]	0.06[d]	−52.9[d]	...	...
CG	6.5	0.35	−6.3	0.53	no CO
G249.0 + 73.7	4.4	1.63	−0.6	1.71	no CO
G124.1 + 71.6	10.0	1.10	−11.4	1.09	no CO
G107.4 + 70.9	3.8	0.52	−29.9	1.13	no CO
G99.3 + 68.0	6.1	0.65	−26.6	1.06	no CO
G86.5 + 59.6	5.2	0.68	1.3	...	...
	6.6	2.04	−39.0	...	...
CG	40.3	2.72	−39.0	3.89	no CO
G90.0 + 38.8	5.0	0.71	−23.9	0.88	−25
G94.8 + 37.6	8.7	0.76	−23.3	0.95	−24
G81.2 + 39.2	3.3	1.16	3.5	...	...
	6.1	0.54	9.7	...	...
CG	6.2	1.70	3.5	1.71	no CO
G86.0 + 38.3	5.0	1.06	−43.4	1.21	no CO
G25.1 − 67.7	10.4	1.30	−1.6	1.42	−8

[a] In the case of multiple H I velocity components, the last line is the condensed Gaussian, labeled CG, adopted for purposes of statistical analysis. For CO, a number indicates the velocity; "no CO" indicates that the cloud was observed with no detection; and "not observed" indicates that the cloud was not observed.

[b] N(H I, total) is the total H I column density difference between the on and off positions. It may differ from that in the fitted Gaussians, which do not always represent the profile perfectly.

[c] Questionable detection.

[d] This component was discarded for the reason discussed in the text.

320

velocity shocks permeated G230.1−28.4 and that, at the present, the shocks have dissipated. G230.1−28.4 is only two degrees away from G228.0−28.6, another cloud with prominent 12 μm emission. G228.0−28.6 has two prominent Gaussians in the position-switched profile. One is broad, one is narrow, and they are separated by 13.8 km s^{-1}, equal to 4.1 times the sound velocity of the broad Gaussian if its width is due to thermal motions alone.

This pair of Gaussians is what we would expect for a shock: because molecules are present, cooling times are short (McKee and Hollenbach 1980), so shocked gas should be cold and have narrow line width; the unshocked gas should reside in the broad Gaussian component. The narrow Gaussian of G228.0−28.6, which is the recently shocked component in this interpretation, has nearly the same V_{LSR} as that of G230.1−28.4 and is only 4% broader. Both clouds exhibit CO emission in the narrow Gaussian component, as would be expected because molecules form in shocks. In this interpretation, we predict that the small-scale structure in G228.0−28.6 (the northern cloud in Fig. 1) contains the narrow shocked Gaussian, while the diffuse structure contains the broad Gaussian.

The IR properties of these two clouds are similar. G230.1−28.4 has $S_{12}/S_{100} = 0.121 \pm 0.010$, the highest in the sample, and G228.0−28.6 has $S_{12}/S_{100} = 0.086 \pm 0.010$, the third highest. Their values of S_{60}/S_{100} are nearly identical, ~0.20. Below, we argue that the S_{12}/S_{100} values are high because of shock processing of grains.

In summary, the close physical proximity of these two clouds, the close similarity of their narrow H I Gaussian components, the CO in their narrow H I components, and the similarity of their IR emission argue that these clouds are intrinsically similar. The seemingly clear indication of shocked gas in G228.0−28.6 then argues that G230.1−28.4 also contains recently shocked gas.

b) Molecular Content and Kinematics

Draine and Anderson (1985, hereafter DA) have presented theoretical calculations of the four IRAS band intensities for several grain distributions of the Mathis, Rumpl, and Nordseick (1977; hereafter MRN) type. A larger population of small grains (of radius $a \lesssim 100$ Å) and a smaller population of large grains ($a \gtrsim 1000$ Å) both lead to increases in S_{60}/S_{100}. They also consider different intensities of the interstellar radiation field, which they take as linearly proportional to χ; $\chi = 1$ near the Sun. We expect $\chi = 1$ for all of our clouds, because they should all be nearby and, in addition, none are located near bright stars. For $\chi = 1$, DA calculate that the IRAS band 4 flux density per hydrogen nucleus, S_{100}/N_H, is close to 1 MJy sr^{-1}/ 10^{20} cm^{-2} for all grain models. The careful observational study of de Vries, Heithausen, and Thaddeus (1987), which considers not only H I but also H_2, concludes that the ratio is indeed well defined for one high-latitude region, and close to the theoretical ratio with $dS_{100}/dN_H = 1.0 \pm 0.4$ MJy sr^{-1}/ 10^{20} cm^{-2}. Within the errors, this is equal to the value of 0.77 MJy sr^{-1}/10^{20} cm^{-2} found by Boulanger and Perault (1988) for the Galactic polar caps.

Figure 4 presents S_{60}/S_{100} versus S_{100}/N_{HI} for the observed clouds, along with DA's theoretical results for the unmodified MRN distribution with $\chi = 1$, which is denoted by an open star.[2] The star lies near the lower left corner of the observed points. Theoretically, S_{100}/N_{HI} varies with χ in an approximately linear fashion. Theoretically, S_{60}/S_{100} depends mainly on the grain size distribution: large values are caused by a larger population of small grains and a smaller population of very large grains.

Several of our points lie much too far to the right of the filled

---

[2] In the figures, the N_{HI} used is that of the sum of the Gaussian components. If we had instead used the total of the position-switched measurement, our results would differ only in detail.
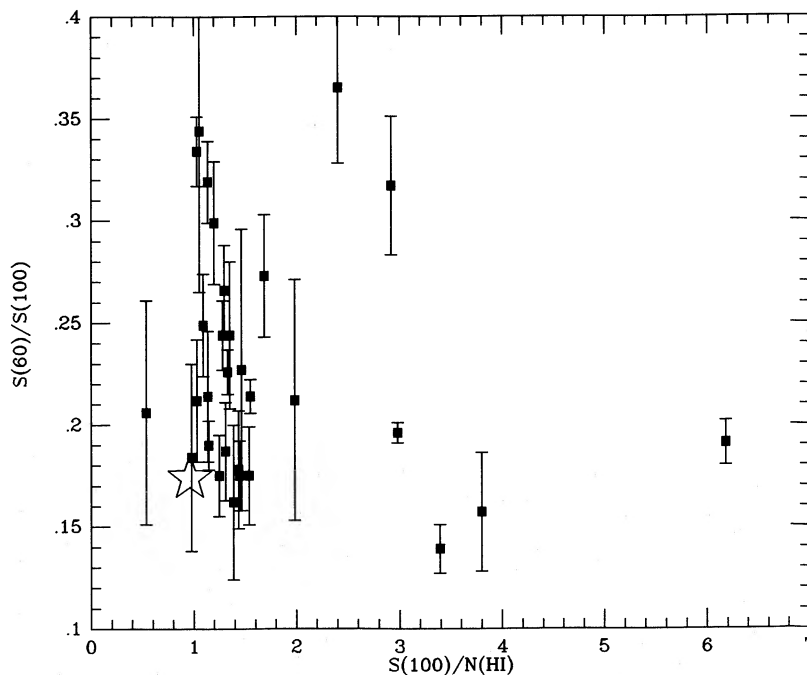
FIG. 4.—S_{60}/S_{100} vs. S_{100}/N_{HI}. N_{HI} reflects only the H I in the Gaussians deemed to be associated with a cloud in the position-switched H I line profile. DA's theoretical calculation for the unmodified MRN distribution, with $\chi = 1$, is shown by the open star symbol.

star. A simple explanation is that we plot the value of S_{100} per H *atom* and some of the gas may be molecular. This possibility is supported by our CO observations: each of the four clouds with the highest values of S_{100}/N_{HI} exhibit CO emission. This 100% detection rate compares with a 37% detection rate for the whole ensemble of CO-observed clouds. The 37% is a lower limit for the true fraction of clouds that actually do contain CO, for two reasons: one, the CO distribution is patchy, and we might have observed at the wrong position; two, the CO may be present at signal levels below our sensitivity, which was typically ~0.4 K or less. Nevertheless, these statistics seem compelling. We should also emphasize that some of our clouds have very low total column densities, much lower than in ordinary molecular clouds; in these cases, it is possible that H_2 exists in the absence of CO, or vice versa.

We conclude that large values of S_{100}/N_{HI} are a result of a significant fraction of the H nuclei residing in H_2. In other words, S_{100}/N_{HI} is a "H_2 indicator"—the departure from its value in purely atomic clouds is a measure of the H_2 content of a cloud. The value in purely atomic clouds appears to be ~1.3 MJy sr^{-1}/10^{20} cm^{-2} from Figure 4, which is close to the DA–predicted value of 0.96 MJy sr^{-1}/10^{20} cm^{-2}. The theoretically unpredictable presence of H_2 means that, if we were to replot the data in Figure 4 and replace the horizontal axis by S_{100}/N_H, the points could shift to the left by arbitrary amounts. As a result, we cannot make any conclusions whatsoever concerning the value of χ. The most straightforward assumption is that $S_{100}/N_H \approx 1$ for all points—i.e., that $\chi = 1$. In this case, the value of S_{60}/S_{100} can depend only on the grain size distribution.

The presence of H_2 in some of these clouds is surprising because they have such small column densities. Perusal of Tables 1 and 2 shows that the four clouds having the largest values of S_{100}/N_{HI} have S_{100} ranging from 1.14 to 2.40 MJy

sr^{-1}. Adopting the convenient de Vries *et al.* (1987) ratio $dS_{100}/dH_H = 1.0$ MJy sr^{-1}/10^{20} cm^{-2}, this implies N_H ranges from 1.14 to 2.40 × 10^{20} cm^{-2}, where again N_H refers to the column density of hydrogen *nuclei*, and corresponds to $E(B-V)$ of 0.02–0.04 mag. This extinction is well below the UV-observed threshold of ~0.08 for the presence of significant amounts of H_2 (Savage *et al.* 1977). One might argue that this estimate of $E(B-V)$ is too small, because it has been derived from the "position-switched" value of S_{100} and would not include a possible component from a very large envelope around the clouds. However, such a contribution is small for these four clouds, for two reasons. First, an envelope should not contain H_2 and the total *non–position*-switched H I column densities are all smaller than 3.1 × 10^{20} cm^{-2}, which corresponds to $E(B-V) = 0.05$ mag. Second, the non–position-switched (i.e., background) 100 μm intensity for these clouds is not significantly larger than that for the other clouds. Thus, the *total* column density is so low that even if *all* of the gas along the line of sight resides close to a cloud, one does not expect the cloud to contain significant amounts of H_2.

Figure 5 exhibits the correlation of S_{100}/N_{HI} with DELTAV, the "internal velocity difference" parameter for a cloud. With only one exception, S_{100}/N_{HI} is large only for DELTAV $\lesssim$ 7 km s^{-1}. This argues that quiescence is required for the formation and retention of H_2 in these low column depth clouds.

Figure 6 exhibits the dependence of S_{100}/N_{HI} on V_{LSR}. Points having $|V_{LSR}| \gtrsim 30$ km s^{-1} exhibit systematically low values of S_{100}/N_{HI}. In other words, rapidly moving clouds do not contain H_2. These clouds must have attained their large $|V_{LSR}|$'s by being shocked. Thus, we conclude that H_2 molecules are destroyed by fast shocks. We cannot accurately specify the required shock velocity, both because we measure only one component of the total velocity vector and because the cloud may have been decelerated after having been
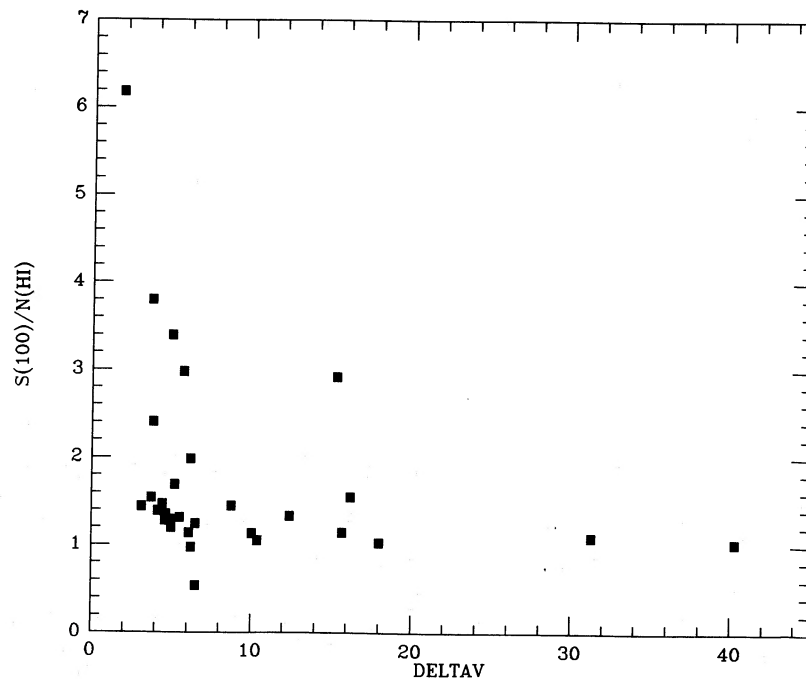
FIG. 5.—S_{100}/N_{HI} vs. DELTAV. As discussed in the text, the departure of S_{100}/N_{HI} from a value of roughly unity is a measure of the H_2 content of a cloud, and DELTAV is a measure of the internal velocity differences within a cloud.
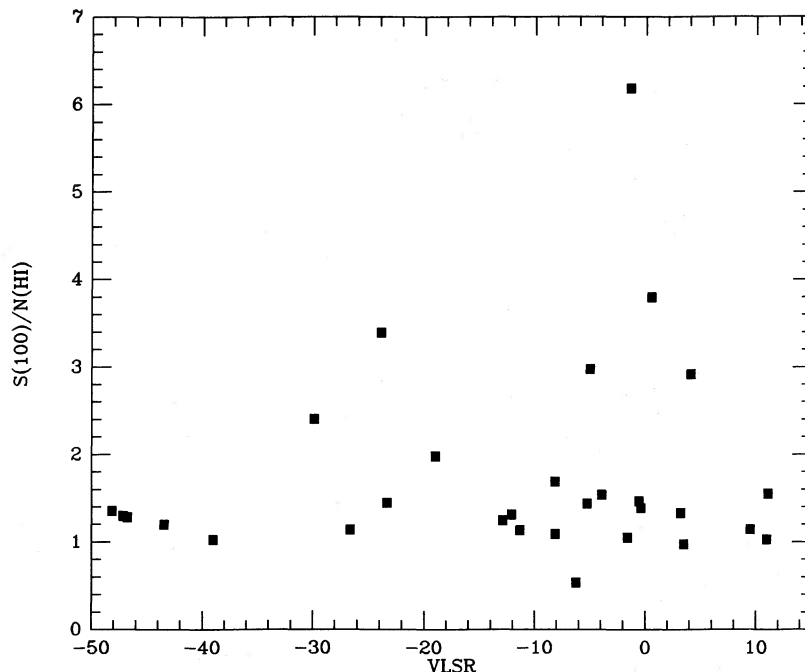
FIG. 6.—S_{100}/N_{HI} vs. V_{LSR}. As discussed in the text, the departure of S_{100}/N_{HI} from a value of approximate unity is a measure of the H_2 content of a cloud, and V_{LSR} is the LSR velocity of the main Gaussian component.

shocked. These results are in good qualitative, and perhaps even quantitative, agreement with theoretical predictions (Hollenbach and McKee 1980).

c) Fast Shocks and Large Grains

DA predict that large values of S_{60}/S_{100} occur with distributions containing few large grains or many small grains, or both, i.e., that S_{60}/S_{100} is a grain size indicator. Figure 7 exhibits

S_{60}/S_{100} versus V_{LSR}. In Figure 7, points having $|V_{LSR}| \gtrsim 30$ km s^{-1} exhibit systematically large values of S_{60}/S_{100}. This is not a strong correlation, in that other low-$|V_{LSR}|$ points also have large S_{60}/S_{100}'s. Nevertheless, it is significant: S_{60}/S_{100} for $|V_{LSR}| > 29$ km s^{-1} is 0.29 ± 0.02, while that for the other points is 0.21 ± 0.01 (errors are error of the mean; see Bevington 1969). These clouds must have attained their large $|V_{LSR}|$'s by being shocked. The effect of large velocities on S_{60}/S_{100} is
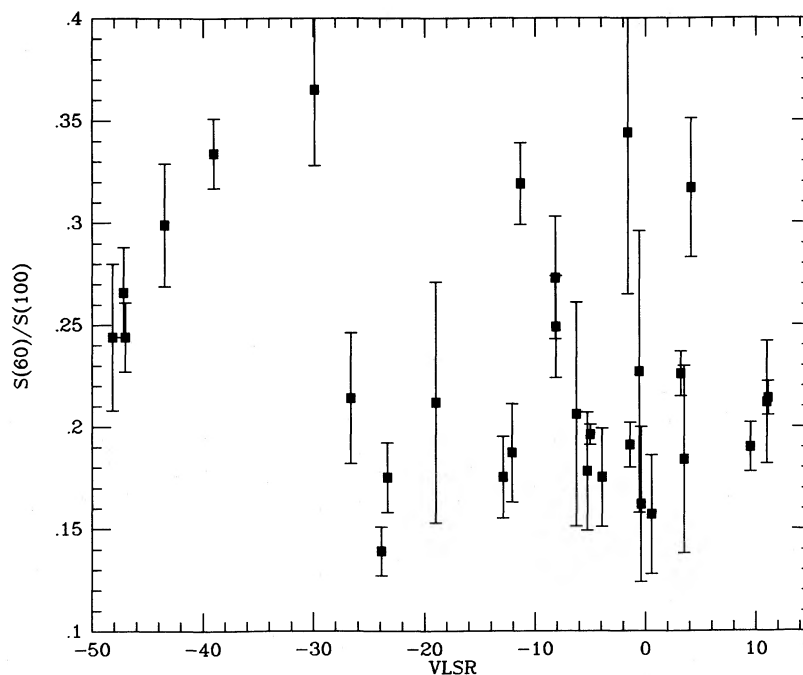
FIG. 7.—S_{60}/S_{100} vs. V_{LSR}. As discussed in the text, S_{60}/S_{100} is a grain size distribution indicator, and V_{LSR} is the LSR velocity of the main Gaussian component.

corroborated by Tables 1 and 2, which show that G86.5 + 59.6, the only cloud with DELTAV > 30 km s^{-1}, has one of the highest values of S_{60}/S_{100}, 0.33.

We conclude that fast shocks modify the grain size distribution. The existence of low-$|V_{LSR}|$ points with large S_{60}/S_{100} does not contradict this conclusion, because these low-$|V_{LSR}|$ clouds may have been strongly shocked in the past, and subsequently slowed down, as apparently happened for G230.2 − 28.4 (see § IVa, above). Figure 7 suggests that shock velocities of at least ∼30 km s^{-1} are required to modify the grain size distribution. However, the value of 30 km s^{-1} is a lower limit, both because we measure only one component of the total vector and because clouds may have been decelerated after having been shocked.

The conclusion that fast shocks observably modify the grain size distribution is in accord with the theoretical predictions of Seab and Shull (1983). They find significant grain destruction only for shock velocities above ∼40 km s^{-1}. Furthermore, they predict that large grains, with $a > 500$ Å, are preferentially affected; these are just the grains that produce most of the 100 μm radiation. The more recent theoretical predictions of McKee et al. (1987) suggest that the grain distribution in a 50 km s^{-1} shock is less size-selective than found by Seab and Shull, and also that the change of the distribution is less drastic overall, by a factor that depends sensitively on the magnetic field strength. Owing to uncertainties in the original shock velocity, our results are also in agreement with McKee et al.

d) Kinematics and the 12 μm–emitting Very Small Grains (VSGs)

The 12 μm *IRAS* emission from diffuse interstellar matter has been discussed earlier by Boulanger et al. (1985) and Weiland et al. (1986). It is commonly interpreted to be caused by very small polycyclic aromatic hydrocarbon grains (PAHs; Léger and Puget 1984; Omont 1986). It is certainly true that PAHs exist, because their spectral features match those

observed in M82 and NGC 2023 (Désert et al. 1986). However, as emphasized by Patrick Thaddeus (private communication), there may be other 12 μm–emitting grain components, such as C_{60}, dubbed "Buckminsterfullerene" (Kroto et al. 1985; Kroto and McKay 1988), and chain molecules such as polymerized formaldehyde, which has been found in comet Halley (Mitchell et al. 1987).

There may be a whole spectrum of very large molecules, which may alternatively be called very small grains (VSGs). Below, we find that these VSGs dominate the IR emission of some clouds, and would require a disturbingly large fraction of the interstellar Carbon be resident in PAHs if PAHs were the sole component of VSGs. Thus it would be comforting if VSGs contained other elements in addition to carbon. So despite the apparently widespread belief that PAHs are the *sole* component of VSGs, we believe that other types of VSG may contribute, and in order not to prejudice the issue we shall refer to the 12 μm–radiating particles as VSGs.

Figure 8 exhibits S_{12}/S_{100} versus V_{LSR}. This plot seems to be largely a scatter diagram. However, S_{12}/S_{100} tends to be large for $|V_{LSR}| \lesssim 10$ km s^{-1}: the average value outside this range is 0.043 ± 0.003, while that inside the range is 0.071 ± 0.005. This indicates that VSGs are destroyed in velocity fields ∼10 km s^{-1} or greater. This velocity is a lower limit because we measure only the line-of-sight component. However, they are apparently not completely destroyed: even for $|V_{LSR}| > 10$ km s^{-1}, the average S_{12}/S_{100} is ∼2.5 times larger than the highest value predicted by DA for distributions not containing VSGs.

Figure 9 exhibits S_{12}/S_{100} versus DELTAV. The points appear to be distributed randomly. However, there is one common group of points that has a relatively large S_{12}/S_{100}, although the difference is only of marginal statistical significance. This group consists of the single point with the narrowest DELTAV and the group of four points with DELTAV between 15 and 20 km s^{-1}; the average S_{12}/S_{100} for these five points is 0.089 ± 0.009. The four with large DELTAVs have
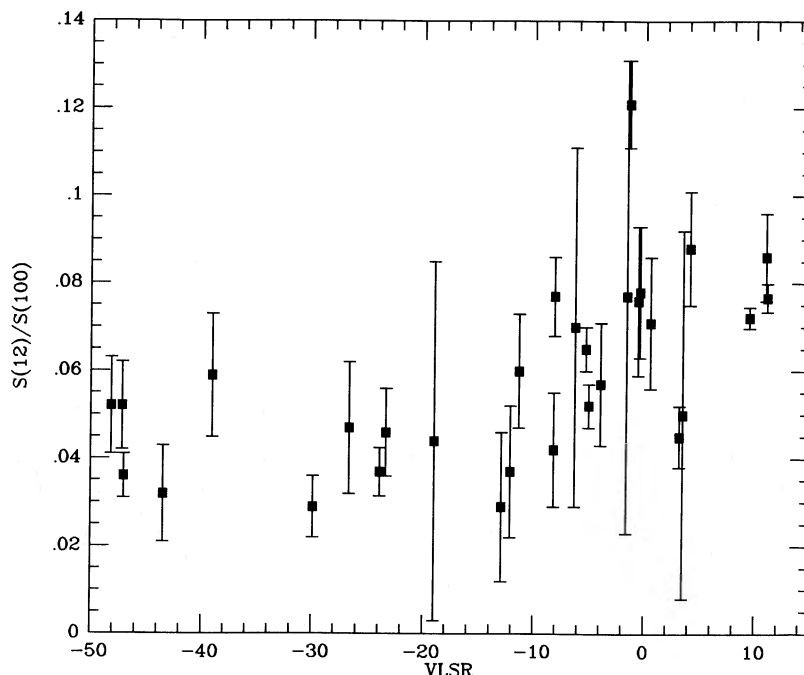
FIG. 8.—S_{12}/S_{100} (the VSG indicator) vs. V_{LSR} velocity of the main Gaussian component
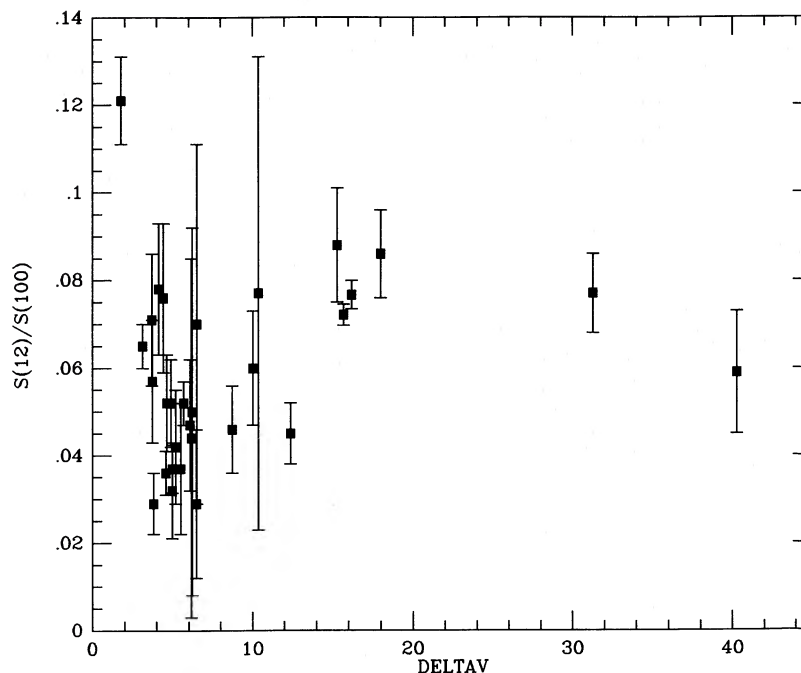
FIG. 9.—S_{12}/S_{100} (the VSG indicator) vs. DELTAV. DELTAV is a measure of the internal velocity differences within a cloud.

multiple velocity components; the fifth, G230.1 − 28.4 with the narrow DELTAV, has recently been shocked by the same collision that G228.0 − 28.6 is currently undergoing, during which time it had DELTAV $\approx$ 16 km s^{-1} (§ IVa above). These five points indicate that VSGs are produced by cloud collisions for velocities $\sim$ 16 km s^{-1}. This is a lower limit because the total collision velocity must be larger than the line-of-sight component that we measure. This conclusion is very tentative, not only because of the scatter in Figure 9 but also because these five points represent only three independent clouds.

The large value of S_{12}/S_{100} in G228.0 − 18.8—and, in particular, the larger value in G230.1 − 28.4—is direct evidence, in a specific case, that VSGs form while a cloud is being shocked. Above, in § IVa, we argued that the former cloud is currently being shocked, and the latter has finished being shocked; thus, we imagine VSG formation has had a longer time to act in G230.1 − 28.4. To estimate an upper limit on the time scale for VSG formation, we simply take the linear diameter of G228.0 − 28.6 divided by the velocity difference of its two Gaussian components. The angular size of the G228.0 − 28.6, as estimated from the *IRAS* data, is $\sim$ 50′. The 13.2 km s^{-1} feature is located in the Eridanus H I shell (Heiles 1976), which is likely to lie at a distance of $\sim$ 400 pc (Reynolds and Ogden 1979). This translates into a time scale of 0.3 Myr and a mean H I volume density $\sim$ 12 cm^{-3}. The time scale for formation of VSGs must be smaller than this if the VSG population in G228.0 − 28.6 is to rival that in G230.1 − 38.4.

In summary, Figure 9 suggests that VSGs are formed by shocks with velocity $\sim$ 16 km s^{-1}, while Figure 8 suggests that they are destroyed by shocks with velocity $\sim$ 10 km s^{-1} or greater. This is seemingly contradictory, but not necessarily so because both numbers are lower limits. The specific case of G228.0 − 28.6 and G230.1 − 38.4 supports the suggestion of VSG formation and allows us to make a crude estimate of the time scale for VSG formation. One possible conclusion from this somewhat confusing situation is probably that VSGs are

formed in shocks in the 10–20 km s^{-1} velocity range and destroyed at slightly higher velocities. There are only a very few clouds for which S_{12}/S_{100} is as low as that predicted by DA, which implies that VSGs exist in *all* clouds.

Duley and Williams (1984) and Omont (1986) have pointed out that the planar PAHs are rather weakly bound to ordinary graphite grains. Theoretically, this implies that PAHs can be produced in low-velocity shocks by being split off of an ordinary grain by collisions of the grain with either H atoms, H_2, or other graphite grains. This is expected to occur in shocks of moderate velocity, of order 10 km s^{-1}. With marginal significance, our data appear to support these theories—and as a corollary, that most of the 12 μm emission is indeed produced by PAHs.

e) MRN Grains versus VSGs

The total mass in VSGs required to explain the observed amounts of 12 μm emission is nontrivial. If VSGs are exclusively PAHs, Boulanger and Perault (1987) estimate that 15% of all C must reside in PAHs for $S_{12}/S_{100} = 0.046$. In G230.1 − 28.4, S_{12}/S_{100} is 2.6 times higher, implying that 40% of all C must reside in PAHs in this cloud. According to DA, ordinary MRN grains must contain $\sim$ 58% of the total interstellar carbon. The sum of these fractions is 98%, and although this sum is not very accurate it implies severe depletion of gaseous carbon. The contribution from other types of VSG that do not primarily contain carbon could relieve this situation. Buckminsterfullerine, which has a high cross section per C atom because it is hollow, is an interesting solution.

Another way to appreciate the overall importance of VSGs is to consider Figure 10, which presents S_{12}/S_{100} versus S_{60}/S_{100}. The flux density S is obtained from the *IRAS*-observed flux F by dividing by the equivalent bandwidths of the filters that defined the bands, assuming that $S \propto v^{-1}$. The *IRAS*-observed flux ratio, F_{12}/F_{100}, can be recovered from the quoted S_{12}/S_{100} by multiplying by 13.6. Thus, whenever
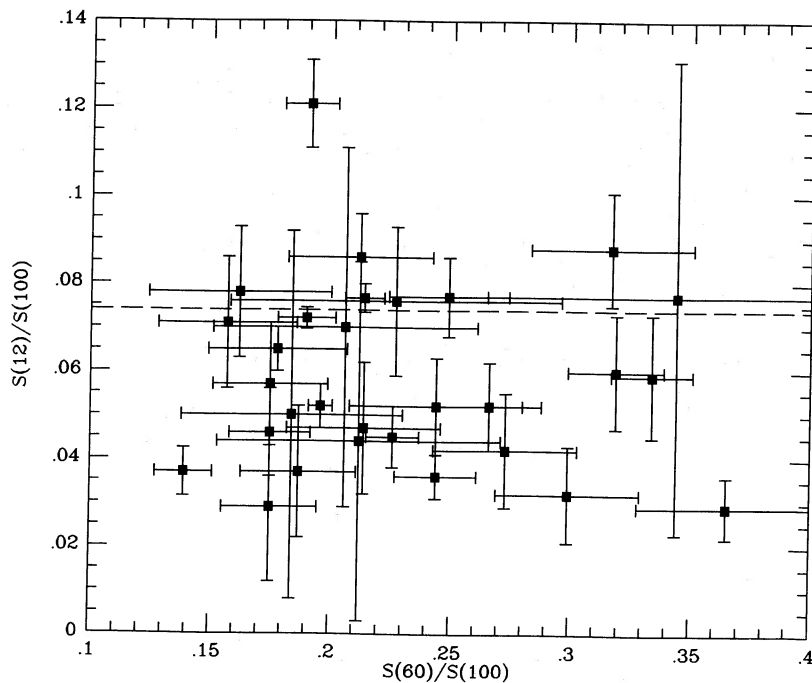
FIG. 10.—S_{12}/S_{100} vs. S_{60}/S_{100}

$S_{12}/S_{100} > 1/13.6 = 0.074$, the *IRAS*-measured 12 μm flux exceeds the 100 μm flux. On Figure 10, we have drawn a dashed line for this value of S_{12}/S_{100}: any cloud above the dashed line emits more power in the 12 μm *IRAS* band in the 100 μm band. Many points lie near the dashed line, and the point for G230.1−28.4 lies well above it. In this cloud, the VSGs emit more power than the MRN grains. Therefore, they must absorb more starlight than the MRN grains: their total UV absorption cross section must exceed that of the MRN grains. This is remarkable, because the effective absorption cross section for small particles is much smaller than the geometric cross section.

In Figure 10, there is no apparent correlation between S_{12}/S_{100} and S_{60}/S_{100}. There is no apparent trend for the two ratios to be correlated. Thus, we cannot conclude that VSGs result from the preferential destruction of large grains.

V. SUMMARY

We have compared the IR and H I properties, and CO content, of a set of 26 isolated, roughly degree-sized interstellar clouds. We arrive at the following conclusions, which should be regarded as provisional because of our limited sample:

1. We argue that G230.1−28.4, the cloud with the narrowest H I line, has recently been shocked by the same collision that a neighboring cloud, G228.0−28.6, is currently undergoing. The two clouds exibit similar IR properties, and we argue that the shock has modified the grain size distribution.

2. We find that the ratio S_{100}/N_{HI} ranges up to much larger values than predicted theoretically for the ratio S_{100}/N_H, where N_H represents the column density of H *nuclei*. Clouds with the highest such values are observed to contain CO, and we thereby infer that they contain H_2. We conclude that the departure of S_{100}/N_{HI} from the value for purely atomic clouds is a measure of the H_2 content of clouds. Even clouds with low column density, $\sim 2.4 \times 10^{20}$ H-nuclei cm^{-2} or lower, may

contain more H_2 than H I, in contrast both to results obtained from UV absorption line studies of Savage *et al.* (1977) and to theoretical expectation.

3. The [H_2/H I] ratio of a cloud increases as DELTAV, the measure of its internal velocity differences, decreases, as shown by Figure 5. Figure 6 shows that rapidly moving clouds have small amounts of H_2. These results are in accord with the theoretical predictions of Hollenbach and McKee (1980).

4. The dependence of S_{60}/S_{100} on V_{LSR}, shown in Figure 7, implies that fast shocks preferentially destroy large grains or produce small grains, or both. This is in accord with the theoretical predictions of Seab and Shull (1983) and McKee *et al.* (1987).

5. While S_{12}/S_{100} may depend on V_{LSR} (Fig. 8; § IVd) and DELTAV (Fig. 9; § IVd), these dependencies are statistically uncertain and need confirmation by further work. If they are real, the former implies that the 12 μm emitting VSGs are destroyed by shocks with velocity ~ 10 km s^{-1} or greater, and the latter implies that VSGs are formed in shocks with velocity ~ 16 km s^{-1}. Both velocities are lower limits and are therefore not necessarily inconsistent. The specific case of G228.0−28.6 and G230.1−38.4 allows us to make crude estimates of time scales for VSG formation. One possible conclusion from this somewhat confusing situation is that VSGs are formed in shocks in the 10–20 km s^{-1} velocity range, and destroyed at slightly higher velocities. There are only a very few clouds for which S_{12}/S_{100} is as low as predicted by DA, which implies that some component of VSG exists in *all* clouds.

6. Some members of our cloud sample emit more power in the *IRAS* 12 μm band than in the 100 μm band. If VSGs are exclusively PAHs, such clouds must have very large fractions of their total carbon in the form of PAHs. This may argue for the existence of types of 12 μm–emitting VSG that do not primarily contain carbon.

7. Figure 10 exhibits no obvious correlation of S_{12}/S_{100} with S_{60}/S_{100}, suggesting that VSGs are not preferentially from the breakup of large grains.

REFERENCES

Bevington, P. R. 1969, *Data Reduction and Error Analysis for the Physical Sciences* (New York: McGraw-Hill).
Boulanger, F., Baud, B., and van Albada, G. D. 1985, *Astr. Ap.*, **144**, L9.
Boulanger, F., and Perault, M. 1987, *Ap. J.*, **330**, 964.
Colomb, F. R., Pöppel, W. G. L., and Heiles, C. 1980, *Astr. Ap. Suppl.*, **40**, 47.
de Vries, H. W., Heithausen, A., and Thaddeus, P. 1987, *Ap. J.*, **319**, 723.
Désert, F. X., Boulanger, F., Léger, A., Puget, J. L., and Sellgren, K. 1986, *Astr. Ap.*, **159**, 328.
Draine, B. T., and Anderson, N. 1985, *Ap. J.*, **292**, 494 (DA).
Duley, W. W., and Williams, D. A. 1984, *M.N.R.A.S.*, **211**, 97.
Heiles, C. 1976, *Ap. J. (Letters)*, **208**, L137.
Heiles, C., and Habing, H. J. 1974, *Astr. Ap. Suppl.*, **14**, 1.
Hollenbach, D. J., and McKee, C. F. 1980, *Ap. J.*, **241**, L47.
Johnson, H. M. 1986, *Ap. J.*, **309**, 321.
Kroto, H. W., and McKay, K. 1988, *Nature*, **331**, 328.
Kroto, H. W., Heath, J. R., O'Brien, S. C., Curl, R. F., and Smalley, R. E. 1985, *Nature*, **318**, 162.

Léger, A., and Puget, J. L. 1984, *Astr. Ap.*, **137**, L5.
Magnani, L., Blitz, L., and Mundy, L. 1985, *Ap. J.*, **295**, 402.
Mathis, J. S., Rumpl, W., and Nordseick, K. H. 1977, *Ap. J.*, **217**, 425 (MRN).
McKee, C. F., and Hollenbach, D. J. 1980, *Ann. Rev. Astr. Ap.*, **18**, 219.
McKee, C. F., Hollenbach, D. J., Seab, C. G., and Tielens, A. G. G. M. 1987, *Ap. J.*, **318**, 674.
Mebold, U., Cernicharo, J., Velden, L., Reif, K., Crezelius, C., and Goerigk, W. 1985, *Astr. Ap.*, **151**, 427.
Mitchell, D. L., *et al.*, 1987, *Science*, **237**, 626.
Odenwald, S. F., and Rickard, L. J. 1987, *318*, 702.
Omont, A, 1986, *Astr. Ap.*, **164**, 159.
Reynolds, R. J., and Ogden, P. M. 1979, *Ap. J.*, **229**, 942.
Savage, B. D., Bohlin, R. C., Drake, J. F., and Budich, W. 1977, *Ap. J.*, **216**, 291.
Seab, C. G., and Shull, J. M. 1983, *Ap. J.*, **275**, 652.
Verschuur, G. L. 1975, *Ann. Rev. Astr. Ap.*, **13**, 257.
Weiland, J. L., Blitz, L., Swek, E., Hauser, M. G., Magnani, L., and Rickard, L. J. 1986, *Ap. J. (Letters)*, **306**, L101.

CARL HEILES, WILLIAM T. REACH, and BON-CHUL KOO: Astronomy Department, University of California, Berkeley, CA   94720